Spectral Emissivities and Temperatures of Burning Iron as Single Particles or Groups of Particles

Yuan Yao[a*], Di Chang[a], Aidin Panahi[a,b], Yiannis A. Levendis[a*]

[a]*Mechanical and Industrial Engineering Department, Northeastern University, Boston, MA, USA*
[b]*Chemical Engineering Department, Worcester Polytechnic Institute, Worcester, MA, USA*

Abstract

This manuscript reports on the combustion of powdered iron, for the purpose of utilizing it as an environmentally friendly circular energy carrier. The conducted research investigated the spectral emissivity and temperature of iron particles, burned either individually or in groups. Combustion experiments were conducted under high heating rates in an externally-heated drop tube furnace. The pressure was atmospheric and the axial temperature was nearly-constant at ~1350 K. The oxidizer gas contained 15-100% oxygen in nitrogen diluent. Iron particles were sieve-classified in the 44-53 μm range. Results showed that, depending on the oxygen concentration, and consequently the particle temperature, the average spectral emissivities of single burning particles varied between 0.18 and 0.46, in the 600-1000 nm wavelength range. Corresponding temperatures of single particles varied between 2300 K and 2800 K, increasing with increasing oxygen concentration in the gas. In the case of groups of iron particles burning in air at different particle number densities, average spectral emissivities were found to be in the range of 0.42-0.45, with the upper value associated with denser particle clouds. Corresponding peak temperatures of particle burning in groups were found to be in the range of 2160 K to 2100 K, with the lower value attributed to denser particle clouds.

Keywords: Emissivity; Combustion; Iron; Spectrometer; Temperature

* Corresponding authors:

y.levendis@northeastern.edu

Yao.yuan@northeasten.edu

1. Introduction

Metals, among all elements, can generate the highest volumetric heat release when burned, making them exceptionally dense sources of energy [1-4]. Iron (with an energy density of 41 MJ/liter) is abundant on earth and can be utilized as a carbon-free fuel [5-7]. In powder form, iron can be dispersed in air, ignited and burned to generate heat in a powerplant. The combustion products of iron primarily consist of iron oxides, which can be collected and reduced back to iron in a specialized process, enabling them to be burned again. This makes iron a candidate for circular fuel utilization, offering a means to store and transport energy.

This research focused on the critical properties of spectral emissivity and temperature of powdered iron particles and examined their behavior when burned both as isolated particles and as groups of particles. Combustion experiments were conducted in a laboratory-scale drop tube furnace (DTF) at elevated particle heating rates and temperatures, simulating conditions typically found in pulverized-fuel suspension-type utility boilers.

In recent years, several studies have reported on the combustion of iron particles, see for instance [8-16]. Some studies reported on flame temperatures [10-12]. Julien et al. [10] investigated flame structures and particle combustion regimes of fine polydisperse micron-sized particles (d~2.2 μm), burning in hybrid fuel mixtures of methane and iron, using a modified Bunsen burner. Particle concentrations varied from 0-350 g/m^3. In the hot post-flame gas (2200 K) at an excess oxygen concentration of 5%, particle spectrometric temperatures were in the broad neighborhood of 2600 K, depending on the particle concentration. The iron particles were assumed to behave as gray bodies, implying that their emissivity was assumed to have no dependence on the wavelength for the region of interest in that study (500-700 nm).

McRae et al.[11] investigated stabilized, flat iron carbonyl particle flames of polydisperse micron-sized particles (d~2.5 μm) using a hot counter-flow burner. Assuming again that the iron particles behaved as gray bodies, they reported average particle temperatures of 2630 K and 2781 K in 30%O_2/Ar and 40%O_2/Ar mixtures, respectively using the same spectrometer as Julien et. al [10]. Palečka et al.[12] observed discrete flame propagation regime of iron particles (d~33 μm) suspended in a flame tube under microgravity using spectrometry. Combustion occurred in 20%O_2/Xe and 40%O_2/Xe gases, and respective temperatures were ~2500 K and ~2800 K. However, a comparison of such experimental measurements with thermodynamic prediction of the temperature of diffusively burning particles agreed only with the former condition. In the case of the latter condition, the authors concluded that the emission spectra may not have been gray. Tang et al [13] investigated the flame propagation of iron dust (3–27 μm) suspensions in tubes under microgravity. Based on typical iron flame spectra registered by spectrometry, they obtained the temperature of the burning particles by linear fitting of the spectral intensity to Planck's law. They concluded that the emitting particles were practically gray in the wavelength range of 500–850 nm. Ning et al. [14], ignited single particles of different sizes in the range of 26-54 μm using a laser beam in ambient temperature O_2/N_2 gases, with oxygen concentrations in the range of 13-50%. Temperatures of ignited particles varied between 2150 K and 2720 K, depending on the particle size and oxygen concentration in the gas. Those authors also used the gray body assumption because, they mentioned, there is lack of data on spectral emissivity of iron and iron oxide at the concerned temperature range. Panahi et al. [15] measured temperature-time histories of individual 45-53 μm iron particles burning in air using a drop-tube furnace. An average peak particle temperature of 2506 K was measured with three-wavelength ratio pyrometry, again making the gray-body radiation assumption. This assumption was drawn

based on the good agreement of the three different two-color temperatures of the three-wavelength pyrometer. In recent work by Hameete et al. [16] burned 32-54 μm iron particles in air. Particles were carried in a capillary flow of nitrogen (9 m/s) and were introduced to a coaxial air flow (1 m/s) of air preheated to 1015 K. Under the resulting high slip velocities, the authors reported particle temperatures in air to be in the broad neighborhood of 2800 K.

Krishnan et al.[17] reported the average iron spectral emissivity to be 0.35 for the liquid melt at 1890 K in the wavelength range of 300 to 1700 nm. Kobatake et al. [18] reported the spectral emissivity of liquid iron to be ~0.38 in the broad neighborhood of the iron melting point (1600-1950 K), in the wavelength range of 780-920 nm. They reported only small departures from graybody radiation. Muller et al. [19] burned iron rods in pure oxygen and reported that at high temperatures (well above the 1811 K melting point of iron) two superimposed phases exist in the melt, iron (Fe) and wustite (FeO). Below 2350 K the two phases are distinct and immiscible, whereas above this temperature the two phases are mixed. The emissivity of molten iron was taken as 0.35±5%, based on the work of Krishnan et al. [17], whereas the emissivity of liquid iron oxide at λ=1064 nm was measured to be 0.7±10% at the maximum temperature of 3400 K. Goett et al.[20] and Mitchell et al. [21] reported that in the wavelength range 650-850 nm, the average spectral emissivity of melted steel (S235), shielded from combustion by argon gas, decreased with increasing temperature in the range of 1900-2100K.

This work burned iron particles under high heating rates and high gas temperatures. Both isolated single particles and groups of particles were burned. Temperatures of single particles and groups of particles were measured by accounting for the variation of spectral emissivity with wavelength, i.e., without making the gray-body radiation assumption. In the case of

single iron particle combustion, temperatures and spectral emissivities were measured in different O_2/N_2 concentrations, to assess the effect of the oxidizer gas. In the case of group particle combustion, temperatures and spectral emissivities were measured in air while the particle number density in the furnace was varied. In the case of single particle combustion, temperature was obtained by three different methods: (**i**) photo-spectrometry, which measured simultaneously spectral emissivity and temperature at a large number of wavelengths in the range of 600-1000nm, (**ii**) three color pyrometry which measured lumped particle temperature at three distinct wavelengths, incorporating the spectrometrically-measured emissivities and (**iii**) a digital camera which measured two-dimensional temperature of particles based on the RGB method and again incorporating the aforementioned spectral emissivities. In the case of group particle combustion only methods (**i**) and (**iii**) were implemented, i.e., photo-spectrometry and digital camera, employed simultaneously.

This research endeavored to answer the following questions. (a) What are the spectral emissivities and temperatures of single iron particles burning in air and in gases with different oxygen-nitrogen concentrations, in a wavelength range of interest in pyrometry of burning solid particles? (b) Does the particle temperature differ by either accounting for the spectral emissivity dependence on wavelength or ignoring such dependence, i.e., making the gray-body radiation assumption? (c) How do iron particles burn in groups and how does this mode of combustion affect the average emissivity and temperature of the group, as well as the temperature of individual particles in the group?

2. Materials and Methods

2.1 Materials

Iron particles were supplied by TLS Technik GmbH & Co in Germany. A scanning electron microscopy (SEM) photograph in Fig.1 reveals spherical/spheroidal particles in the narrow size range of 45-53 µm. The particle size distribution of these particles, based on examining several SEM photographs is also included in Fig.1.

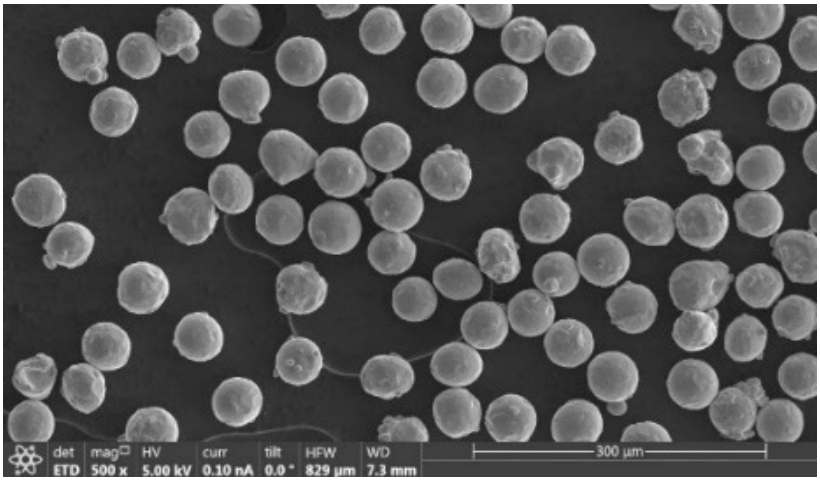

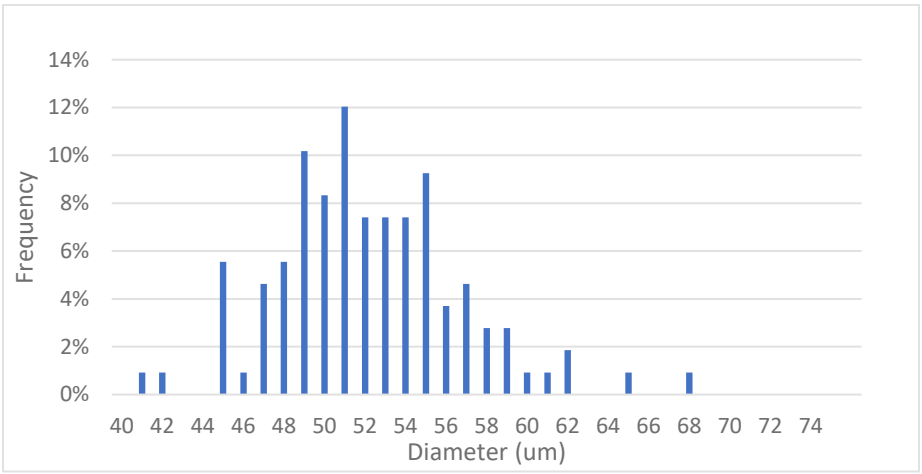

Figure 1. Scanning Electron Micrograph (SEM) of iron particles in the 45-53 µm nominal sieve size and their actual measured size distribution.

2.2 *Experimental Apparatus and Methods*

Combustion of iron particles took place in an electrically heated laminar-flow drop-tube furnace (DTF), manufactured by *Applied Test Systems* (*ATS*), depicted in Fig. 2. The furnace was fitted with a transparent quartz tube to facilitate combustion observations. In all experiments, the furnace wall temperature was set at 1400 K; the gas temperature at the furnace centerline was measured with radiation-corrected thermocouples to be ~1350 K for most of the length of the 25 cm long radiation zone. The heating rate of the particles was determined to be in the range of 10^4-10^5 K/s; details are given in Refs. [15, 22].

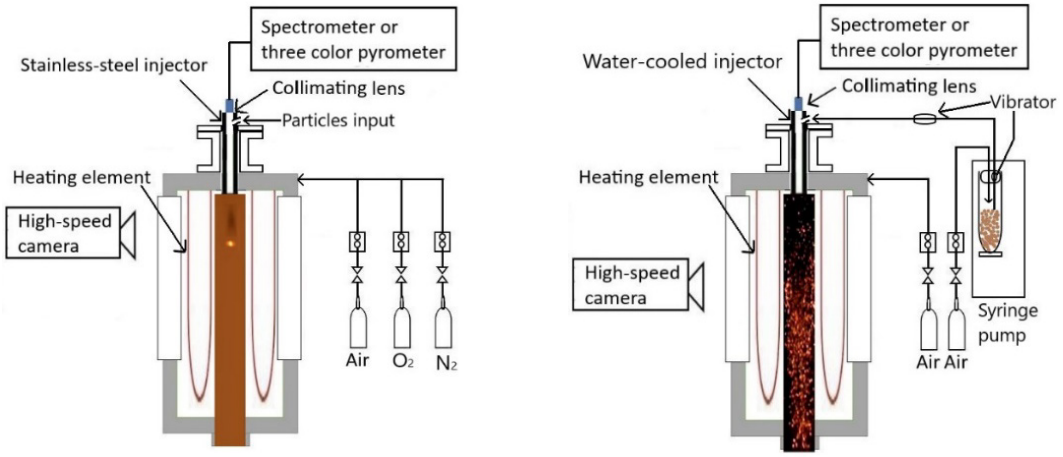

Figure 2. Schematic illustration of the drop tube furnace. Left: Single particle combustion setup. Right: Group particle combustion setup.

In single particle experiments, the flowrate of gas to the furnace was set at 1 l/min. Five different oxygen concentrations in nitrogen gas were implemented: 15% O_2, 21% O_2 (air), 35% O_2, 50% O_2 and 100% O_2. In these single particle experiments, no gases were introduced through the furnace injector. A very small quantity of iron particles was scooped by the tip of a beveled needle syringe and released into the furnace injector by a gentle tap. Therefrom, free-falling particles entered the DTF, where they ignited and burned. Combustion was

monitored in real time. When only one particle was detected burning in the DTF its combustion record was saved.

In particle group combustion, the flowrate of air was set at 2.2 l/min through the furnace injector and 0.8 l/min through the annulus between the injector and the furnace tube, totaling 3 l/min. Streams of particles with introduced into the furnace with a programable syringe pump, *KDS Model 200 Series_5600-002REVH*, through a thin metal tube, vibrated to prevent jamming. Two different settings of the syringe pump resulted in two different mass flow rates of particles in the DTF. To distinguish these two conditions, which were implemented in this investigation, one was termed *dilute* and the other was termed *dense*. Such characterizations are arbitrarily defined herein, based on cinematographic evidence, still frames of which are presented in Figure 6, Section 3.2 of the manuscript.

The average particle number density ($PND = N/V$) in the visible section of the transparent drop tube furnace (through the observation windows depicted in Fig. 2) was obtained by counting particles in 15 different photographic frames recorded by the camera. In this expression, V is the total furnace volume occupied by the group as defined in Ref. [23], and N is the estimated total number of particles in the group. The interparticle distance was also calculated based on the PND as follows: $L = (V/N)^{1/3} = (1/PND)^{1/3}$. The assumption made herein is that the burning particles are evenly distributed in a 3-dimensional Cartesian mesh, and each particle stays at the center of the mesh unit. The side length of the mesh unit is taken as the inter-particle distance L [23].

2.3 Spectrometer Operation and Calibration

The spectrometer used for this purpose was an AvaSpec-2048 manufactured by *Avantes* coupled to the top of the particle injector with a 1 m long optical cable (C-UVIR600-1-BX, 600 µm UV/IR broadband fiber (200-2500 nm)). During the combustion experiments, light from burning particles was focused on the fiber by an inverted collimating lens (Oriel, 1 l-mm diameter, 19-mm focal length). To accept only parallel rays and also minimize reflected furnace radiation climbing the injector's inner walls (upon multiple reflections) (a) the injector was black passivated and (b) a pinhole was used between the lens and the fiber. The position of the lens was fixed, but both the pinhole and the optical fiber could be moved axially relative to the lens and against each other, thus allowing fine tuning of the light collection system during experiments. Details of this lens/pinhole setup are provided in Fig. 3 of Ref. [24]. The spectrometer incorporated a 16-bit Analog to Digital (A/D) converter to realize raw format pixel values between 0 and 65535 non-dimensional radiation intensity counts in the wavelength range of 600-1000 nm. Integration times for measured signals were set at 10 ms to warrant sufficient signal strengths.

The monochromatic spectral radiation intensity of a graybody, $I_b(\lambda)$ in $[\frac{\mathrm{W}}{\mathrm{m}^3}/\mathrm{sr}]$ of surface temperature, T_s, is given by Planck's law, Ref [24]:

$$I(\lambda) = \varepsilon_\lambda \frac{c_1}{\lambda^5\left(e^{\frac{c_2}{\lambda T_s}}-1\right)} \tag{1}$$

Where c_1, c_2 are Planck's first and second constants. As shown in Equation 1, the spectral radiation intensity of a graybody object depends on its spectral emissivity ε_λ. In this work surface temperature, T_s and the spectral emissivity ε_λ of burning iron particles were calculated concurrently with the Newton iteration method [25]:

$$|f|^2 = \sum_{j=1}(I_m(\lambda_j) - I(\lambda_j)) = \sum_{j=1} \left(\mathrm{I_m(\lambda_j)} - (\mathrm{a_0 + a_1\lambda_j + a_2\lambda_j^2 \ldots + a_4\lambda_j^4}) \frac{\mathrm{C_1}}{\lambda_j^5 \left(e^{\frac{\mathrm{C_2}}{\lambda_j T_s}} - 1 \right)}\right) \quad (2)$$

In this expression, the spectral emissivity ε_λ is taken as a fourth-order polynomial function: $\varepsilon_\lambda = a_0 + a_1\lambda_j + a_2\lambda_j^2 \ldots + a_5\lambda_j^4$ (the solution is similar if a higher order polynomial is used).

The polynomial expression used in this work was proposed in Refs. [26, 27] and it was then used in previous work by the authors to successfully measure the temperatures of platinum-based thermocouples, see Figs 14 and 15 in Ref. [25]. Thereafter, it was again used successfully to measure the temperature and the emissivity of various types of heated platinum thermocouples [28]. Finally, it was used in measurements of biomass flames [29]. Based on this validation, this expression was again adopted in this work.

The quantity $I_m(\lambda_j)$ represents the measured monochromatic spectral radiation intensity. The quantity $|f|^2$ represents the absolute mean square error between the measured intensities and the calculated monochromatic spectral radiation intensities at different wavelengths. Once $|f|^2$ reaches the minimum value, the respective surface temperature and the polynomial function of spectral emissivities represent the final calculated results.

The spectrometer was calibrated with a pre-calibrated gas-filled tungsten filament lamp, model *S6–100* acquired from *Pyrometer LLC* (New Jersey, USA). The lamp was positioned at the bottom of the furnace, mounted in the upright position. A section of the tungsten filament, specified by the manufacturer, was viewed through two pinholes, placed in series, and a mirror tilted at 45 degrees, see Ref. [24]. The diameter of the smaller pinhole was 500 µm. The following apparent temperature values for the lamp filament (T_a) were provided by *Pyrometer LLC* at the wavelength of 0.65 µm, at different electrical current inputs: 2073 K, 2173 K, 2273 K, 2373 K, and 2473 K. Based on these temperatures, the following true

temperatures (T_t) of the lamp: 2249 K, 2369 K, 2489 K, 2612 K, and 2735 K were calculated using Eq. 13 of Ref.[24] in conjunction with corresponding emissivity values for tungsten published by De Vos [30] Calibration of the spectrometer was done by converting the raw intensity data from units of "count" to units of $\frac{\mathrm{W}}{\mathrm{m}^3}/\mathrm{sr}$ using a calibration function, R_λ:

$$R_\lambda = f(\text{wavelength}) = \frac{\varepsilon_{\text{lamp}}(\lambda_j) \times I_{b,\text{lamp}}(\lambda_j)}{I_{\text{lamp}}(\lambda_j)} \quad (3)$$

In this expression, $\varepsilon_{\text{lamp}}$ is the emissivity of the lamp filament; $I_{b,\text{lamp}}$ is the calculated blackbody intensity of the lamp filament at T_t (in units of $\frac{\mathrm{W}}{\mathrm{m}^3}/\mathrm{sr}$) from Planck's law (the product of these two terms is given by Eq. 1); whereas I_{lamp} is the measured intensity in units of "count". The calibration function R_λ is plotted in Fig. 3a versus the wavelength of observation (600-1000 nm). The effect of different temperatures on the R_λ function is relatively small, hence the average value of R_λ may be applied to all the temperatures of this study. Once the calibration function R_λ was obtained, the raw intensities (in counts) of the burning iron particles were multiplied by R_λ to convert their signals from counts to the units of $\frac{\mathrm{W}}{\mathrm{m}^3}/\mathrm{sr}$.

$$I_{\text{m}} \times R_\lambda \times AF = I'_m(\lambda_j) \quad (4)$$

In this expression, I_{m} is the intensity of a combustion event measured by the spectrometer in the units of counts; I'_m is the intensity of the combustion event in the units of $\frac{\mathrm{W}}{\mathrm{m}^3}/\mathrm{sr}$ and AF is an area factor which depends on the ratio of the luminous areas during the experiment and during the calibration.

$$AF = \frac{Area\ of\ the\ calibration\ pinhole}{Luminous\ top\ area\ of\ a\ single\ particle\ or\ a\ group\ of\ particles} \quad (5)$$

The diameter of the calibration setup pinhole was 0.5 mm. The luminous projected areas were obtained with the high-speed camera and average values were taken during the combustion of 20 different particles or groups of particles. In the experiments where single particles were injected in the DTF, the viewed cross section luminous areas of individual particles had average diameters in the order of 0.1 mm, based on photographic evidence, see Ref. [15]. In experiments where streams of particles were injected in the DTF, particles burned in groups (clouds). In the case of clouds which were labeled *dilute* their viewed cross section luminous areas had diameters of ~ 0.61 mm. In the case of clouds which were labeled *dense* their viewed cross section luminous areas had diameters of ~1.22 mm. It is estimated that a ~14% uncertainty in the emissivity measurement was caused by this method. The view angle of the calibration lamp filament through the pinholes was the same as the view angle of the burning particles so relevant corrections were not applied. The accuracy of the method was deemed satisfactory when tested in the past against thermocouple readings in a flame [28].

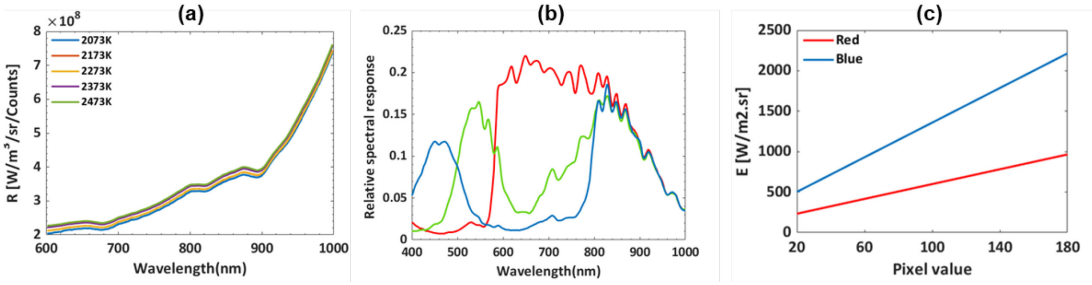

Figure 3. (a) Spectrometer calibration function R_λ for different apparent lamp filament temperatures, observed in the wavelength range of 600-1000 nm. (b) Relative spectral response curves of the RGB bands of the high-speed electronic camera. (c) Calibration curves for red and blue channels of high-speed electronic camera.

2.4 Electronic camera and calibration

Two-dimensional temperatures of burning both single particles and groups of particles in this study were measured by high-speed *Edgetronic* 8GB color camera, operated at a shutter speed

of 1/1000s and a frame rate of 1000 frames/s. In each combustion event, the recording duration was 11 s and the Audio Video Interleave (AVI) raw format and QuickTime video format (MOV) high-quality video files were recorded. The camera has three channels for recording signals, labelled as Red, Green, and Blue. The raw signal for each channel has 0-255 luminance levels; however, to prevent saturating the signal a neutral density filter was added, thus the luminance level was kept under 200. This method followed this investigation is different than camera-pyrometry methods, as it employed the entire wavelength spectrum from 400-1000 nm. Use of such a broad spectral range permitted comprehensive temperature assessment, offering a reliable means of temperature determination for complex and dynamic systems like high temperature fast moving objects, like free falling iron particles, exemplified by these burning particles. The camera measured the amount of radiation intensity from combustion events that reached its imaging sensor and outputted an image with pixel values (RGB) that correspond to the input radiation intensity. The particle radiation intensity E_i, over the observed wavelength range for combustion events at different surface temperatures, T_s, captured by the camera is given by the following expression [25]:

$$E_i = \int_{\lambda_1}^{\lambda_2} \eta_i \cdot \tau \cdot \varepsilon_\lambda \cdot \frac{c_1}{\lambda^5\left(e^{\frac{c_2}{\lambda T_s}}-1\right)} d\lambda = \mathrm{f}(pixel\ value_i) \quad i = R, G, B\ channel \tag{6}$$

In this expression, $\eta_i(\lambda)$ represents the relative spectral response for each channel, supplied by camera's manufacturer, shown in Fig. 3b; T_s is the surface temperature; ε_λ is the spectral (monochromatic) emissivity, which was taken from the spectrometry; τ is the shutter time of the camera; and $E_i = \mathrm{f}(pixel\ value_i) = a \times pixel\ value_i + b$ is the calibration fitting curve that transfers the $pixel\ value_i$ from i channel to radiation intensity E_i. Pixels representing regions with temperatures at or lower than the furnace temperature (1400 K) were not accounted for in the calculation of combustion temperatures. The wavelength range of

297 emissivity measurements for the spectrometer was set to 600-1000 nm. However, because the
298 spectral response of the camera is in the range of 400-1000 nm, spectral emissivities in the
299 400-600 nm portion of the spectrum were extrapolated. Using different emissivities at that
300 wavelength range has no noticeable result on the temperature values (less than 1 degree K
301 difference). The surface temperature T_s is obtained from the solution of Eq. (6).

302 To calibrate the high-speed camera, the tungsten filament lamp was placed at an identical
303 distance from the camera as that of the particle combustion events in the furnace. The response
304 wavelength of the R channel is the strongest, whereas the B channel is the weakest, in the
305 temperature range of 1300-3000 K. The responses of the R and B channels were selected for
306 the temperature measurements. The calibration curves for converting raw data pixel values to
307 radiation intensities E_i in the R and B channels of the camera are shown in Fig. 3c.

308 *2.5 Three-color pyrometer and calibration*

309 The three-color optical pyrometer of Levendis, Estrada and Hottel [24] was also used to
310 measure the temperature of burning single particles. Light from burning particles was
311 transmitted to the pyrometer [24]. The two-color ratio method was used to calculate three
312 temperatures based on the particle radiation intensity signals obtained from the three channels
313 of the pyrometer (S_{999}/S_{810}, S_{810}/S_{640}, S_{999}/S_{640}). Often the three different detector signals result
314 in somewhat different temperatures based on the uncertainties in the emissivities, which are
315 listed in Tables, 1 and 2. In this analysis we retained signals which had the best agreements
316 among the three temperatures. The details of the method and pyrometer's calibration were
317 documented in [15, 24, 31].

318

319

3. Results

3.1 Combustion of single particles

Spectral emissivities and temperatures of iron particles burning at different gas conditions were measured by photo-spectrometry. Particles were treated as lumped light sources. Values reflect temporal averaging over the burntime of particles. In addition, three-wavelength pyrometry of burning particles provided high-resolution temporal temperature distributions, over the entire burntime of individual particles. The emissivities obtained by the spectrometer were utilized in the pyrometric temperature measurements. The measured spectral emissivities of burning iron particles, averaged over a dozen particles in each case, were 0.46, 0.38, 0.18 0.21 and 0.21, respectively in 15% O_2, 21% O_2 (air), 35% O_2, 50% O_2, and 100% O_2. The spectral emissivity of particles decreased with increasing oxygen concentration in the gas. However, in most cases, the spectral emissivity of the iron particles varied little in the wavelength range of 600-1000 nm. Spectrometric particle temperatures were found to increase with the oxygen concentration with as follows: 2292 K, 2431 K, 2554 K and 2758 K and 2780 K, respectively in 15% O_2, 21% O_2 (air), 35% O_2, 50% O_2, and 100% O_2. These results are shown in Fig. 4 and are included in Table 1. Values of particle temperatures and emissivities experienced some deviations from their means because of variations of particle diameter in this size cut, surface inhomogeneities and, possibly, their exact locations in the furnace. Above ~50% O_2, the rise of temperature with oxygen concentration moderated significantly with increasing oxygen concentration and reached ~2800 K at 100% O_2. Such moderation in temperature raise with oxygen concentration above a certain threshold was also observed by Ning [14]. Particle temperatures obtained by the spectrometer are representative temperatures in the flame but they are not necessarily peak temperatures, as only a few data

points were taken during the burnout duration of each particle, which typically lasted for 20-40 ms [15].

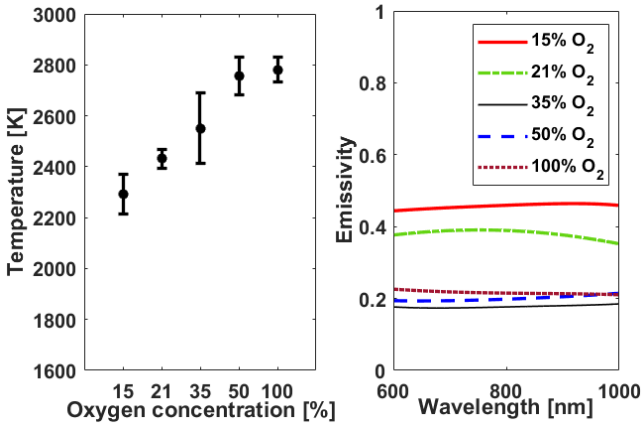

Figure 4. Spectrometric temperatures and emissivities of single iron particles burning in oxygen-containing nitrogen gases.

Pyrometric temperatures were determined both with and without accounting for the variation of the emissivity with wavelength. The validity of the commonly made graybody radiation assumption was investigated. The peak pyrometric temperatures (averaged over at least 10 particles in each case) were as follows: 2394 K, 2505 K, 2689 K, 2836 K and 2827 K, respectively in 15% O_2, 21% O_2 (air), 35% O_2, 50% O_2, and 100% O_2, based on the graybody assumption for the emissivity. These peak particle temperatures were ~100 K higher than the spectrometric average particle temperatures, which is reasonable since the latter were not necessarily peak values. Results showed that the pyrometric temperatures deduced with the graybody radiation assumption differed by as little as 4 K and as much as 37 K from those determined with the graybody radiation assumption. Values of both temperatures are displayed in Table 1.

Two-dimensional camera snapshots of recorded temperature of single particles burning at five different oxygen concentrations in nitrogen are displayed in Fig. 5 and are also included in Table 1. The determination of these temperatures included spectroscopically derived

emissivities. The center portions of these images depict the temperature of the burning solid particles, whereas the lower temperatures at the periphery of the particles most likely correspond to the surrounding nanoparticle cloud. The overall diameters of the nanoparticle mantles (200-300 μm) are in line with those observed by Ning et al. [32]. The peak temperatures from the camera are also in line with the peak pyrometric temperatures.

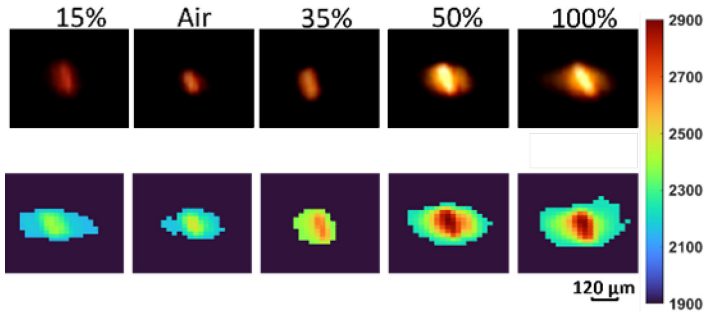

Figure 5. Top Row: photographs of different single iron particles burning in diverse O_2 concentrations in N_2. Bottom Row: corresponding 2-D temperature maps obtained from the green (G) channel of the camera. Images appear slightly elongated due to the particle's high terminal velocity.

Table 1. Average spectrometric temperatures and emissivities of **single particles** of iron and peak pyrometric temperatures (in both cases averaged over 10 particles).

Single iron particles burning in various O_2/N_2 gases					
Gas	**15% O_2**	**Air**	**35% O_2**	**50% O_2**	**100% O_2**
$T_{ave,from\ spectrometer}$ (K)	2292±77	2431±36	2554±131	2758±74	2780±49
$\varepsilon_{ave\ effective}$	0.46±0.04	0.36±0.06	0.18±0.05	0.21±0.01	0.21±0.06
$T_{peak,from\ pyrometer\_graybody}$ (K)	2394±46	2505±56	2689±19	2836±34	2827±60
$T_{peak,\ from\ pyrometer\_non\ graybody}$ K)	2390±45	2467±56	2685±19	2845±34	2824±60
$T_{peak,\ camera}$ (K)	2406±92	2506±59	2637±22	2887±86	2875±56

3.2 Combustion of particles in groups

Based on photographic evidence recorded through the furnace windows and following Annamalai's group particle combustion classification [33], the iron particles within groups appear to burn rather discreetly in both cases labeled as *dilute* or *dense*, as exemplified in Fig. 6. However, it cannot be entirely ruled out that the latter case may have experienced some localized interparticle interactions.

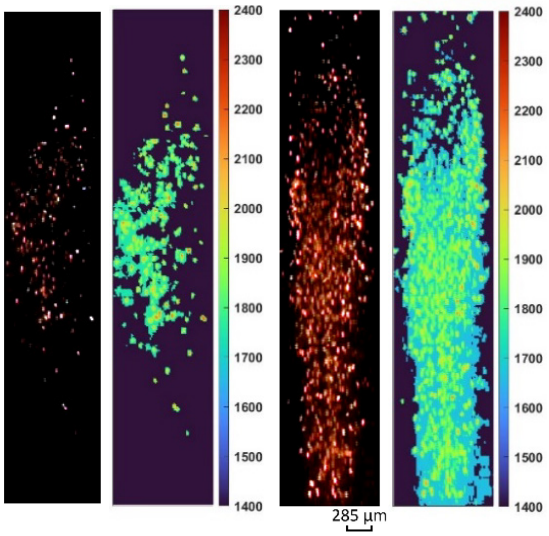

Figure 6. High-speed photography of group iron particle combustion in air with different PND-associated 2-D temperature maps obtained from the green (G) channel. Left: dilute cloud. Right: dense cloud.

The calculated nominal particle number densities ($PND = N_{particles}/V_{gas}$) in these two cases, obtained from 15 different snapshot measurements, were ~35 particles/cm^3 (corresponding to a mass density of ~19 g/m^3) and ~100 particles/cm^3 (corresponding to 54 g/m^3) of furnace volume. Corresponding global equivalence ratios, φ, were calculated based on the PNDs as:

$$\varphi = \frac{\left(m_{Fuel}/m_{Air}\right)_{actual}}{\left(m_{Fuel}/m_{Air}\right)_{stoichiometric}} \quad (7)$$

Where the $m_{Fuel} = \rho_{particle} \cdot V_{particle} \cdot PND = \rho_{particle} \cdot \pi(D^3/6) \cdot PND$, where $\rho_{particle}$ is the density of iron, $V_{particle}$ is the volume of a single iron particle and D is the average diameter of the particles. At the gas temperature of the furnace (T~1350 K), the density of air was taken as 0.00027 g/cm^3. This calculation was performed assuming that the main product of the iron particle combustion under these conditions was a mixture of 50% Fe_2O_3 – 50% Fe_3O_4. The values of the calculated global equivalence ratios are listed in Table 2. Emissivities and temperatures of groups of iron particles burning in air, obtained from spectrometry and electronic camera, are also listed in Table 2 and plotted in Fig. 7.

Table 2. Average temperatures and emissivities of particles burning in **groups** using concurrent measurements with camera and spectrometer, taken over many snaphshots. Peak particle temperatures with camera (10 different frames) are included, as well as particle number densities, mass loadings, interparticle distances and equivalence ratios.

Streams of iron particles undergoing group combustion in air		
	Dilute	**Dense**
$T_{ave,\ spectrometer}$ (K)	2063 ± 96	1929 ± 35
ε_{ave}	0.42 ± 0.039	0.46 ± 0.058
$T_{ave,\ camera}$ (K)	1809 ± 3	1751 ±10
$T_{max,\ camera}$ (K)	2160 ± 27	2103 ± 15
PND (particles/cm^3)	35 ± 5	100 ± 13
Mass loading (g/m^3)	19.1 ± 1.8	54.7 ± 4.3
L (mm)	3 ± 0.1	2.1 ± 0.06
Φ	0.12 – 0.13 (± 0.01)	0.33 – 0.37 (± 0.03)

Both particle number densities in the furnace resulted in higher average emissivities than those of single particles burning in air. As the PND increased from 35 to 100, the emissivity also increased from 0.42 to 0.46, which values are close to the emissivity of the 15% O_2/85% N_2 condition for single iron particles. Examining the 2D temperature colormap in Fig. 6, a large domain of temperatures (~1850 K for a dilute cloud, ~1750 K for a dense cloud) is seen between burning particles. This is attributed to the hematite nanoparticle aerosol dispersed in the interparticle space which, may have contributed to refraction or scattering of radiation emanating from burning particles.

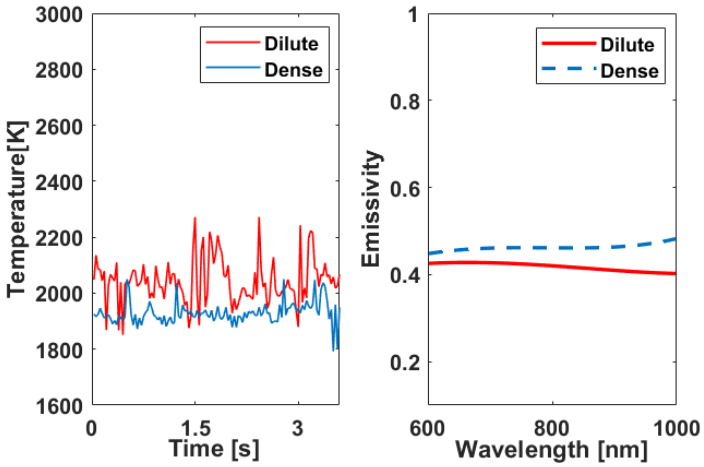

Figure 7: Spectrometric temperature and emissivity for iron particle dilute and dense clouds, burning in 1350 K air.

4. Discussion

Single Particles: At the wavelength range of interest (600-1000 nm) for high-temperature combustion of iron in furnaces, the representative values for the effective spectral emissivity of isolated iron particles were in the vicinity of 0.36, in air, at corresponding particle temperatures in the neighborhood of 2500 K. This emissivity value is in the range of spectral emissivities (0.35-0.38), measured by Krishnan et al. [17] and Kobatake et al. [18] in similar wavelength ranges, for iron pools heated at or above their melting temperature. This similarity of values suggests the presence of molten iron at the surface of the burning particles as conversion to FeO is taking place, although emission peaks of this suboxide of iron, in the neighborhood of 590 nm [34, 35], were not significantly pronounced in the collected raw spectroscopic data, perhaps they were overwhelmed by combustion-emitted radiation. The particle temperatures are in line with those reported by Panahi et al. [15] in prior experiments in the laminar flow DTF of this laboratory and by Ning et al. [32] in a different experimental setup. However, recent work by Hametee et al. [16] reported higher particle combustion temperatures (2700 K) in air. The authors explained those higher values based on the high velocity gradient between the injected particles and a parallel stream of hot oxidizing gas in their burner. The resulting slip velocity may have facilitated the gas phase transport of oxygen to the surface of the burning particles, and this effect may have resulted in higher temperatures by a variety of phenomena mentioned in Ref. [16]. To the contrary, in the laminar flow reactor used herein, where Reynold numbers were in the order of unity, the presence of the nanoparticle cloud surrounding the burning particles could have played a role in the radiation released by the oxidizing particle surface. Hematite aerosols may absorb light in the visible and near infrared spectrum. In the wavelength range of interest to this study, there have been reports that the real refractive index of collected hematite aerosols is ~2.75 and the imaginary

refractive index is in the range of 0-0.2, the combined value being 2.75 - 0.2i. Such values have been retrieved from Ref. [36], based on a large body of literature compiled therein on fine particles of hematite. The real component of the refractive index denotes the velocity of light within the material relative to the speed of light in vacuum. It also indicates how much a ray of radiation will be bent, or refracted, when it passes through the material [37]. The imaginary term indicates how much of the radiation is lost due to absorption [37]. For comparison, the index of refraction of the soot has been measured to be 1.57 - 0.56i [38].

During combustion of iron particles, radiation is emitted by both the oxidizing (burning) micrometric particles, by gas phase oxidation of Fe and/or FeO vapors and by nucleating Fe_2O_3 nanometric particles in the proximity of the vaporizing surface. The radiation emitted from the particle's oxidizing surface is possibly attenuated by the surrounding nanoparticle mantle. Sarofim and co-workers [39, 40] provided a method for obtaining the radiation contributions of the burning micrometric coal particles surrounded by burning soot mantles. Extending this method (see Eq. 2 of [39]) to burning iron particles surrounded by hot nanometric iron/suboxide/oxide particles, the contributions of the radiation from these two components were calculated. The surface temperature of a single micrometric particle burning in air, was assumed to be 2500 K and the temperature of the nanoparticle mantle was taken as 2000 K, based on the 2D temperatures shown in Fig. 5. To calculate the radiative contributions, it was assumed that 4% of the iron particle mass was vaporized in air and converted to nanoparticles, based on current measurements in this laboratory and past reports in [35], consisting of 100 nm diameter spherules. The nanoparticle mantle diameter enveloping a burning 45 μm particle was taken as 120 μm. The wavelength of observation was taken as 800 nm, the emissivity of the burning iron particle was taken as 0.35 and the refractive index

of the hematite nanoparticle cloud was taken as 2.75 - 0.2i. Under these assumptions, the radiation contribution of the nanoparticle mantle was calculated to account for about one third of the total radiation contribution of the burning particle radiation. In this calculation the particle was assumed to be isothermal and the mantle was also assumed to be isothermal, however the latter assumption is rather questionable. Moreover, the mantle is not necessarily spherical because of the rather high terminal velocity of the micrometric particle. Furthermore, not all of the 4% of the iron particle mass converts instantaneously to hematite nanoparticles; this happens over several milliseconds. Hence, the aforesaid estimated radiation contribution of the nanoparticles may be an upper end estimate. Actual contributions of the mantle to total radiation emission may be less, but they can still be significant.

Finally, fully oxidized nanoparticles that have cooled off to the gas temperature in the furnace may also interfere with the radiative environment in the furnace and affect the measurements. As a burning micrometric iron particle falls fast by gravity, its nanoparticle mantle shapes into a contrail of rapidly cooling nanoparticles, as seen in the dark plume (dark aura) forming behind the falling and burning iron/iron oxide particles. The images in Fig. 8 were taken with backlight photography to observe the nanoparticle plume, whereas the images in Fig. 5 were taken with normal (not backlight) photography. In fact, to be able to observe the nanoparticle contrails together with the burning particles, the latter became mildly overexposed in the photographs in Fig. 8. Clearer shadow photographs are shown in a publication by Ning et al. [32]. Please notice that the dark clouds of nanoparticles in the contrails have most likely already cooled expediently to the temperature of the furnace gas, as expected because of their miniscule size that enhances convective heat loses. Hence, they are not evident in the temperature maps of Fig. 5. Such contrails, particularly from multiple particles in group

particle combustion, could interfere with the pyrometric and spectrometric measurements of temperatures and emissivities.

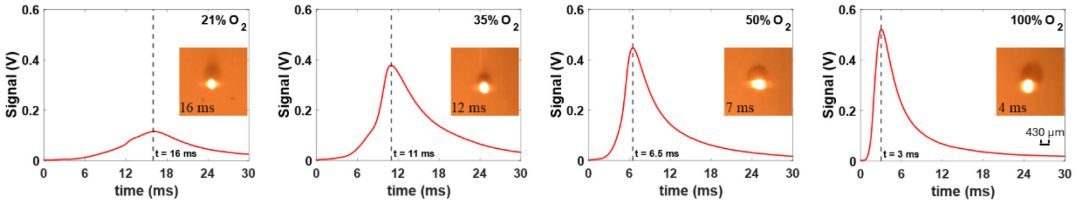

Figure 8: Intensity profiles of burning single iron particles in the DTF at different oxygen concentrations in nitrogen. Photographs of the iron particles show the timing in the burnout profile where the nanoparticle contrails became evident.

As the particle temperature increased at higher oxygen levels, the spectral emissivity decreased. This trend cannot be associated with the increased presence of oxygen in the gas, since O_2 is not known to absorb radiation in the visible and in the near infrared spectra [41, 42]. This trend was also observed by Goett et al. [20] for the spectral emissivity of molten steel at similar wavelengths of observation, albeit in a narrower temperature range. Emissivity values for that steel were a bit lower than the values measured herein, possibly because of its heteroatom content (such as carbon, manganese, phosphorous and silicon). It is noteworthy that this trend of decreasing emissivity with increasing temperature has also been documented in the combustion of coal char particles, see Ref. [43]. Besides the effect of the temperature of the melt on spectral emissivity, there are additional influences in the present experiments. Since the variation of particle temperature was induced by varying oxygen concentration in the gas, there may be contributions by different iron oxides forming in the melt, by different surface structures and by the presence of different amounts of nanoparticles at the periphery of each particle. Such nanoparticles formed by nucleation/condensation of vapors of iron and iron suboxides and oxides at the periphery of burning iron particles, during a fraction of their burnout period. Nanoparticle formation surrounding burning iron particles has been documented in the literature [32]. High-speed photography with the electronic camera and

deduction of 2-D temperature profiles facilitated assessment of temperatures of the burning micrometric particle and the nanoparticle mantle and measurement of its thickness. The size of the mantle appeared to increase with oxygen concentration (see Fig.5), as higher amounts of iron vaporized at the induced higher temperatures increasing the nanoparticle mass flux at the periphery of the particle. The temperature maps in Fig.5 of single particle combustion of iron show distinct high temperature areas at the center, surrounded by lower temperatures areas. Temperatures of the mantle appear to be significantly lower (by a few to several hundred degrees K) than the temperature of the micrometric particles at the center of the images. This is expected as the small nanoparticles oxidize expediently and cool faster to the furnace gas temperature because of their very high surface area to volume ratios.

It should also be noted that the spectral emissivity of single particles is not decreasing monotonically with increasing the oxygen concentration in the gas, but rather decreases from O_2 concentration of 15% to 35% and then it levels off. This behavior may be attributed to factors such as the increased degree of iron oxidation and the formation of different surface structures on the collected iron oxide micrometric particles, and the amounts of nanometric particles generated under different oxygen concentration conditions. Both factors are under current investigation. Finally, the variation of burning particle temperatures deduced with or without the gray radiation assumption of burning iron was observed to be mild (3-38 K).

Streams of Particles: Generally, combustion of fuel particles in groups is influenced by factors such as the particle size, the local oxygen concentrations, which vary both spatially and temporally by the random distribution and motion of the particles, and by multiple heat transfer interactions among the particles [33]. Annamalai et al. [33] reported on mechanisms which occur during combustion of oil droplets and coal/char particles in furnaces, under

various droplets/particle densities and spatial arrangements. Average oxygen concentrations in burning groups of such particles are lower than the ambient oxygen concentrations in the of burning single particles and decrease with increasing particle number density. Iron combustion is expected to follow a similar trend albeit to a lesser extent as they are much less prone to devolatilization. Iron particles burning in groups in the furnace at the globally fuel-lean conditions of this study exhibited discrete particle combustion. However, interactions of their nanoparticle clouds cannot be precluded in this laminar DTF, where mixing was not effective and local oxygen concentrations may have been lower than those of air. As a result, lower average and maximum particle temperatures were measured than those prevailing in single particle combustion; for instance, a 400-550 K drop in average temperatures was recorded. However, such combustion temperatures did not decline linearly with PND, as from single particle combustion to group particle combustion, at PND=35, the average temperature decreased by 400 K, whereas the temperature only decreased by an additional 150 K at PND=100. The effective emissivity of burning particles in groups is also affected by local variations in oxygen concentration which influences local temperatures. It is also likely also influenced the amounts of nanometric fumes (smoke) in the particle stream.

5. Conclusions

This work observed phenomena and assessed important parameters pertaining to the combustion of iron particles in a furnace, both in isolation and in particle groups. Particles experienced high heating rates in the radiation zone of a DTF furnace, ignited in 1350 K oxygen-containing gases and burned to attain high temperatures. Single particles burned at oxygen mole fractions ranging from 15% to 100% in nitrogen diluent, whereas groups of particles were burned in air. Particle emissivities and temperatures were measured with a

photo-spectrometer, while temperatures were also measured with a three-color pyrometer and with an electronic camera. Emissivities of single particles ranged from 0.18 to 0.46, decreasing with increasing oxygen concentration up to somewhere between 35 to 50% [O_2] and remained nearly constant thereafter. Temperatures of single particles exhibited exactly the opposite trend, with peak values ranging from 2390 K to 2845 K, as the oxygen concentration increased. The spectral emissivity of burning iron varied only modestly in the wavelength range of 600-1000 nm. Thus, the graybody assumption appeared to be acceptable for temperature measurement and related numerical simulations. Group particle combustion appeared to occur in discrete mode, however, the overall consumption of oxygen in the group lowered the particle temperatures.

6. Acknowledgment

This work was supported by the US National Science Foundation Grant # DMR-G00008208, Dr. Jonathan Madison, Program Director. Help from Ms. Echo St. Germain to obtain iron particle size distributions is acknowledged.

7. References

[1] Bergthorson J, Goroshin S, Soo M, Julien P, Palecka J, Frost D, et al. Direct combustion of recyclable metal fuels for zero-carbon heat and power. Applied Energy 2015;160:368-82.

[2] Julien P, Bergthorson JM. Enabling the metal fuel economy: green recycling of metal fuels. Sustainable Energy & Fuels 2017;1(3):615-25.

[3] Bergthorson JM. Recyclable metal fuels for clean and compact zero-carbon power. Prog Energy Combust Sci 2018;68:169-96.

[4] Dirven L, Deen NG, Golombok M. Dense energy carrier assessment of four combustible metal powders. Sustainable Energy Technologies and Assessments 2018;30:52-8.

[5] Debiagi P, Rocha RC, Scholtissek A, Janicka J, Hasse C. Iron as a sustainable chemical carrier of renewable energy: Analysis of opportunities and challenges for retrofitting coal-fired power plants. Renewable and Sustainable Energy Reviews 2022;165:112579.
[6] Janicka J, Debiagi P, Scholtissek A, Dreizler A, Epple B, Pawellek R, et al. The potential of retrofitting existing coal power plants: A case study for operation with green iron. Applied Energy 2023;339:120950.
[7] Baigmohammadi M, Prasidha W, Stevens NC, Shoshyn YL, Spee T, de Goey P. Towards utilization of iron powders for heating and power. Applications in Energy and Combustion Science 2023;13:100116.
[8] Wright A, Higgins A, Goroshin S. The discrete regime of flame propagation in metal particulate clouds. Combustion Science and Technology 2016;188(11-12):2178-99.
[9] Li S, Huang J, Weng W, Qian Y, Lu X, Aldén M, et al. Ignition and combustion behavior of single micron-sized iron particle in hot gas flow. Combustion and Flame 2022;241:112099.
[10] Julien P, Whiteley S, Goroshin S, Soo MJ, Frost DL, Bergthorson JM. Flame structure and particle-combustion regimes in premixed methane–iron–air suspensions. Proc Combust Inst 2015;35(2):2431-8.
[11] McRae M, Julien P, Salvo S, Goroshin S, Frost DL, Bergthorson JM. Stabilized, flat iron flames on a hot counterflow burner. Proc Combust Inst 2019;37(3):3185-91.
[12] Palečka J, Sniatowsky J, Goroshin S, Higgins AJ, Bergthorson JM. A new kind of flame: Observation of the discrete flame propagation regime in iron particle suspensions in microgravity. Combust Flame 2019;209:180-6.
[13] Tang F-D, Goroshin S, Higgins A, Lee J. Flame propagation and quenching in iron dust clouds. Proc Combust Inst 2009;32(2):1905-12.
[14] Ning D, Shoshin Y, van Stiphout M, van Oijen J, Finotello G, de Goey P. Temperature and phase transitions of laser-ignited single iron particle. Combustion and Flame 2022;236:111801.
[15] Panahi A, Chang D, Schiemann M, Fujinawa A, Mi X, Bergthorson JM, et al. Combustion behavior of single iron particles-part I: An experimental study in a drop-tube furnace under high heating rates and high temperatures. Appl Energy Combust Sci 2023;13:100097.
[16] Hameete J, Abdallah MS, Thijs LC, Homan TAM, Mi XC, Dam NJ, et al. Particle-resolved hyperspectral pyrometry of metal particles. Combustion and Flame 2024;264:113435.
[17] Krishnan S, Yugawa KJ, Nordine PC. Optical properties of liquid nickel and iron. Phys Rev B 1997;55(13):8201.
[18] Kobatake H, Khosroabadi H, Fukuyama H. Normal spectral emissivity measurement of liquid iron and nickel using electromagnetic levitation in direct current magnetic field. Metall Mater Trans A 2012;43(7):2466-72.
[19] Muller M, El-Rabii H, Fabbro R. Liquid phase combustion of iron in an oxygen atmosphere. J Mater Sci 2015;50(9):3337-50.
[20] Goett G, Kozakov R, Uhrlandt D, Schoepp H, Sperl A. Emissivity and temperature determination on steel above the melting point. Weld World 2013;57:595-602.

[21] Mitchell JA, Ivanoff TA, Dagel D, Madison JD, Jared B. Linking pyrometry to porosity in additively manufactured metals. Addit Manuf 2020;31:100946.
[22] Panahi A, Vorobiev N, Schiemann M, Tarakcioglu M, Delichatsios M, Levendis YA. Combustion details of raw and torrefied biomass fuel particles with individually-observed size, shape and mass. Combust Flame 2019;207:327-41.
[23] Yao Y, Panahi A, Levendis YA. Comparative radiative property measurements of single biomass and coal particles burning at high reactor temperatures. Combust Flame 2024;263:113406.
[24] Levendis YA, Estrada KR, Hottel HC. Development of multicolor pyrometers to monitor the transient response of burning carbonaceous particles. Rev Sci Instrum 1992;63(7):3608-22.
[25] Yan W, Panahi A, Levendis YA. Spectral emissivity and temperature of heated surfaces based on spectrometry and digital thermal imaging–Validation with thermocouple temperature measurements. Experimental Thermal and Fluid Science 2020;112:110017.
[26] Wen C-D, Chr Y-H. The assessment of multispectral radiation thermometry using linear and log-linear emissivity models for steel. Numerical Heat Transfer, Part B: Fundamentals 2010;58(1):40-54.
[27] Wen C-D. Experimental investigation of emissivity of aluminum alloys and application of multispectral radiation thermometry. *International Heat Transfer Conference.* 49408. 2010:867-75.
[28] Yao Y, Panahi A, Levendis Y. Spectroscopic and pyrometric temperature measurements of heated type B and S thermocouples. 2022.
[29] Yan W, Li K, Yu T, Huang X, Yu L, Panahi A, et al. Determination of flame temperatures and soot volume fractions during combustion of biomass pellets. Energy & Fuels 2021;35(3):2313-25.
[30] De Vos JC. A new determination of the emissivity of tungsten ribbon. Physica 1954;20(7-12):690-714.
[31] Bejarano PA, Levendis YA. Single-coal-particle combustion in O_2/N_2 and O_2/CO_2 environments. Combust Flame 2008;153(1-2):270-87.
[32] Ning D, Shoshin Y, van Oijen JA, Finotello G, de Goey Laurentius PH. Critical temperature for nanoparticle cloud formation during combustion of single micron-sized iron particle. Combustion and Flame 2022;244:112296.
[33] Annamalai K, Ryan W, Dhanapalan S. Interactive processes in gasification and combustion—Part III: Coal/char particle arrays, streams and clouds. Prog Energy Combust Sci 1994;20(6):487-618.
[34] Li S, Sanned D, Huang J, Berrocal E, Cai W, Aldén M, et al. Stereoscopic high-speed imaging of iron microexplosions and nanoparticle-release. Optics Express 2021;29(21):34465-76.
[35] Tóth P, Ögren Y, Sepman A, Gren P, Wiinikka H. Combustion behavior of pulverized sponge iron as a recyclable electrofuel. Powder technology 2020;373:210-9.
[36] Go S, Lyapustin A, Schuster GL, Choi M, Ginoux P, Chin M, et al. Inferring iron-oxide species content in atmospheric mineral dust from DSCOVR EPIC observations. Atmos Chem Phys 2022;22(2):1395-423.

673 [37] Shaddix CR, Williams TC. Soot: Giver and taker of light: The complex structure of
674 soot greatly influences the optical effects seen in fires. American scientist
675 2007;95(3):232-9.
676 [38] Sarofim AF. Radiative heat transfer in combustion: friend or foe. *Symposium*
677 *(International) on Combustion.* 21. Elsevier; 1988:1-23.
678 [39] Timothy L, Froelich D, Sarofim A, Beer J. Soot formation and burnout during the
679 combustion of dispersed pulverized coal particles. *Symposium (International) on*
680 *Combustion.* 21. Elsevier; 1988:1141-8.
681 [40] Timothy L, Sarofim AF, Beér JM. Characteristics of single particle coal combustion.
682 *Symposium (International) on Combustion.* 19. Elsevier; 1982:1123-30.
683 [41] Fridovich I. Oxygen: how do we stand it? Medical principles and practice
684 2013;22(2):131-7.
685 [42] Education UCfS. Carbon Dioxide Absorbs and Re-emits Infrared Radiation; n.d.
686 Available from: https://scied.ucar.edu/learning-zone/how-climate-works/carbon-
687 dioxide-absorbs-and-re-emits-infrared-radiation. [Accessed June, 2024.
688 [43] Schiemann M, Gronarz T, Graeser P, Gorewoda J, Kneer R, Scherer V. A correlation
689 between char emissivity and temperature. Fuel 2019;256:115889.

690

691

692